Rev. Energ. Ren. Vol.3 (2000) 49-56

Optical Properties of Microcrystalline Thin Film Solar Cells

N. Senoussaoui, T. Repmann, T. Brammer, H. Stiebig, H. Wagner

Forschungszentrum Jülich GmbH, ISI-PV, D-52425 Jülich, Germany

Abstract – *Mircocrystalline silicon solar cells based on pin and nip layer sequences require an effective light trapping in the near infrared (NIR) to enhance the long wavelength spectral response. Therefore, the effect of interface roughness on the optical properties of microcrystalline pin and nip solar cells was investigated. Based on a detailed analysis of scattering properties of textured substrates the device performance of the realized solar cells deposited by plasma enhanced chemical vapor depositon is discussed. The roughness of the substrates is controlled by a chemical etching step of the ZnO layer, which yields to a root mean square roughness d_{rms} between 10 and 150 nm. The pin diodes deposited on substrates with a roughness exceeding 40 nm show a similar red response although the haze and the angle resolved scattering properties of the substrate differ significantly. It is also found that light trapping in nip structures is less effective than in pin structures.*

Résumé – *Les cellules solaires en silicium microcrystallin basés sur les séquences de couches pin et nip exigent un piégeage effectif de lumière dans le proche infrarouge pour augmenter la réponse spectrale des grandes longueurs d'onde. A cet effet, l'effet de la rugosité de l'interface sur les propriétés optiques des cellules solaires en microcristallin pin et nip est étudié. Basée sur une analyse détaillée des propriétés de diffusion des substrats texturés, la performance du système de cellules solaires réalisées par la méthode de déposition en phase vapeur augmentée par plasma est discutée. La rugosité des substrats est contrôlée par décapage de la couche de ZnO; ce qui engendre une valeur quadratique moyenne de la rugosité d_{rms} entre 10 et 150 nm. Les diodes Pin déposées sur substrats ayant une rugosité supérieure à 40 nm présentent de similaires réponses au rouge, bien que les propriétés du voile atmosphérique et de l'angle de résolution de diffusion des substrats différent d'une manière significative. Il a aussi été trouvé que le piégeage de la lumière dans les structures nip est moins effectif que dans les structures pin.*

Key-Words: Microcrystalline silicon solar cells - pin structure - nip structure - Light trapping – Roughness - pin diodes - Spectral response.

1. INTRODUCTION

The application of textured transparent conductive oxide (TCO) layers to amorphous (a-Si:H) and microcrystalline (µc-Si:H) solar cells based on pin or nip structures is a widely employed method to improve the absorption in thin film solar cells [1-4]. As a result of this texture all subsequent interfaces in the solar cell are also rough. When light strikes a rough interface, scattering occurs. Scattering of transmitted and reflected light prolongs the effective light path in the absorber layer and increases the quantum efficiency considerably, especially beneficial for the long wavelength region.

In the ideal case, the solar radiation is scattered, repeatedly reflected (light trapping) within the solar cell and absorbed after multiple passes through the intrinsic layer which generates the photocurrent. However, a state-of-the-art µc-Si:H solar cell of electronically reasonable thickness (2-3 µm) looses more than 20% (>10mA/cm^2) in short-circuit current due to insufficient light absorption caused by not insufficiently knowledge of the relationship between structural properties, e.g. feature size, and the scattering process.

Light scattering at rough interfaces depends on the wavelength, the interface roughness (δ_{rms}), the morphology, the refractive indices of the media and the light incident angle. It is the purpose of this paper to verify the applicability of already existing theories and to develop functional relationships based on various experimental investigations of rough surfaces in order to discuss the light scattering thin film solar cells. Therefore, two different device structures are investigated and the quantum efficiencies and the solar cell parameters are determined.

Depending on a pin or nip deposition sequence, the microcrystalline layers are deposited on a glass/$ZnO_{textured}$ substrate employed as a transparent front contact or a glass/$ZnO_{textured}$/Ag/ZnO highly reflecting back contact, respectively. The texture of sputtered ZnO:Al film is controlled by a chemical etching step in diluted hydrochloric acid (HCl) [5, 6].

2. EXPERIMENT

The boron doped, intrinsic and phosphorous doped microcrystalline layers were deposited in a multi-chamber deposition system by plasma enhanced chemical vapor deposition (PECVD) under very high frequency condition (VHF) of 95 MHz on glass substrates coated with textured TCO for pin diodes and glass/$ZnO_{textured}$/Ag/ZnO substrates for nip diodes. The i-layers of the diodes were deposited with a silane concentrations in hydrogen ([SiH_4]/([SiH_4]+[H_2]) of 5%.

The thickness of the absorption layer is 1µm. The ZnO films were deposited in a Lesker high vacuum sputtering system. The topology of the rough front TCOs and reflecting substrates were characterized by means of atomic force microscopy (AFM). Optical transmission and reflection were carried out by using a photogoniometer and a spectrometer.

The topology and optical measurements are brought in context through analytic haze calculations. Measurements of the I/V-characteristics were performed under AM1.5 illumination. The QE was measured under a photon flux less than 10^{14} cm^{-2} s^{-1}.

3. RESULTS AND DISCUSSION

3.1 Substrate characterization

Fig. 1 shows the AFM images of textured ZnO used as pin substrates, realized under the same deposition conditions but different etching times (5s, 15s, 25s, and 50s) in diluted hydrochloric acid (HCl). All figures are plotted at the same scale. The etching process of the initially smooth ZnO films

leads to a random rough, crater-like structure and the roughness of the substrates increases with etching time.

The root mean square roughness δ_{rms} as the characteristic vertical surface parameter and the correlation length a_{corr} as the lateral characteristic surface parameter of these ZnO surfaces are shown in table 1. The material properties and the behavior upon etching of the ZnO also depend on the deposition parameters during the ZnO sputtering process [6]. The films were optically characterized by measurements of diffuse and total transmission and reflectance.

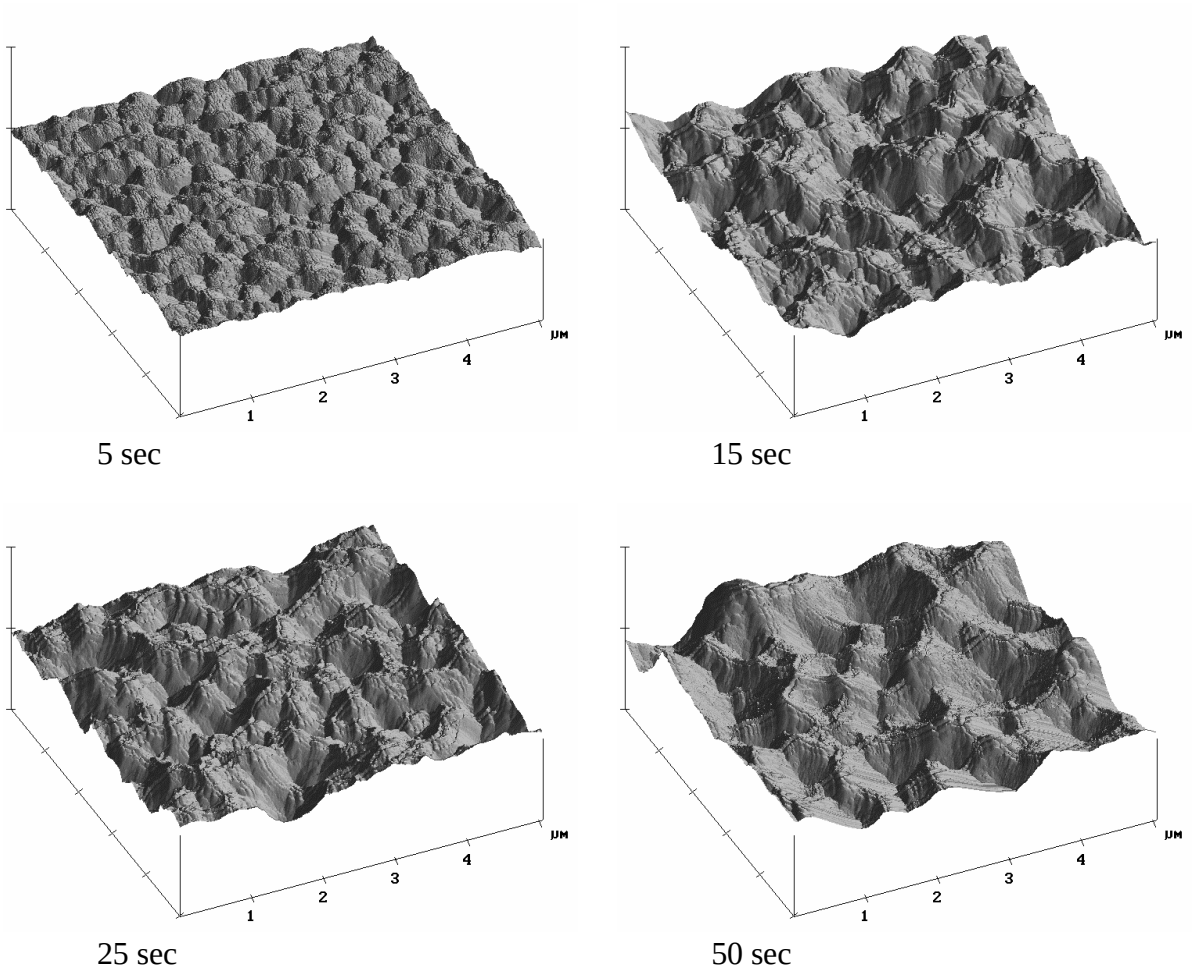

Fig. 1. AFM images of ZnO substrates with different surface roughness due to different etching times of 5s, 15s, 25s and 50s (1 tick = 1µm).

Table 1: Root mean square roughness (δ_{rms}) and correlation length (a_{corr}) in dependence of the etching time of the glass/ZnO substrates

Etching time (s)	δ_{rms} (nm)	a_{corr} (nm)
5	38	133
7	52	169
15	85	304
25	98	336
50	124	451

The effect of the etching time on the fraction of diffusely scattered light can be expressed by the haze which is defined for reflection and transmission by the following equation

$$H_R = \frac{R_{diff}}{R_{total}}, \qquad H_T = \frac{T_{diff}}{T_{total}} \tag{1}$$

where the lower case 'diff' denotes the diffused and 'total' the total reflection or transmission. The measured haze for the etching series is plotted in Figure 2. The fraction of diffused light increases with increasing etching time in the whole wavelength range. In particular, the haze at 800 nm of the 50s etched substrate exceeds 40%. The commonly used analytic function for the haze in reflection in relation to δ_{rms} and the wavelength λ of the incident light is generated by the scalar scattering theory [7].

$$H_R = 1 - \exp\left\{-\left(\frac{4p\,d}{l}\right)^2\right\} \tag{2}$$

This formula is based on the assumptions that (I) the scattering surface is perfectly conducting and that (II) $\delta/\lambda << 1$. To apply this formula to scattering by ZnO surfaces, the glass/ZnO substrates are coated with a thin (200nm) silver layer and only wavelengths $800nm < \lambda < 1100nm$ were considered. By proceeding in that manner ZnO-layers and their roughness can be characterized by means of haze measurement in reflection.

A comparison of the rms-roughness derived from AFM and haze measurement shows a good agreement and confirms the applicability of the chosen techniques and theories. Defining an expression for the haze in transmission from equation (2) for the textured glass/ZnO substrates, an agreement between measured haze in transmission and roughness is not given. Reasonable fits are only achieved for powers in the exponential of larger than 3 instead of 2 and effective roughness smaller by a factor of 1-2.

In figure 3 the Haze of the back contact (air/$ZnO_{textured}$/Ag/ZnO) of the nip substrates with different etching times is shown. The Haze at 800 nm enhances of the 5s etched substrate from 10% to over 80% of the 25s etched ZnO back contact due to the increased roughness of 30 nm and 105 nm, respectively.

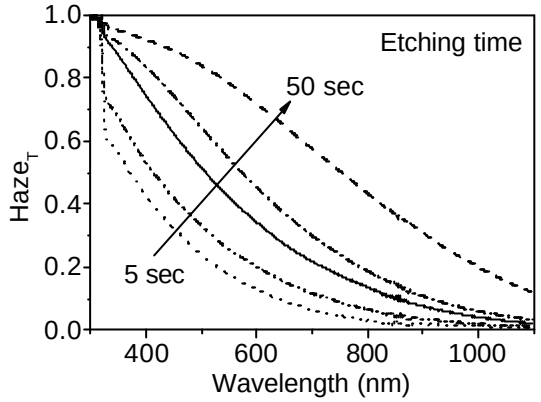

Fig. 2: Haze measured in transmission (air/glass/ ZnO/air) of the pin substrates for different etching times.

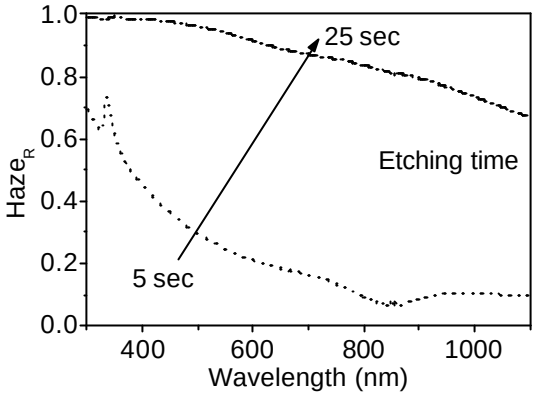

Fig. 3: Haze measurements of back contact (air/ZnO/Ag/ZnO$_{textured}$/glass) for nip substrates with different etching times.

Besides the total integrated scattering (TIS) intensities described by the haze function it is of interest to know the exact angular resolved intensity distribution because total internal reflection occurs only for large angles. Fig. 4 shows the transmitted and reflected intensity per solid angle versus the scattering angle for the multilayer system air/glass/rough TCO/air. For $0<\theta<90°$, the light is incident onto glass and the transmitted intensity is plotted.

For $90°<\theta<180°$, the light is incident onto the textured TCO and the reflection is plotted (λ=684 nm). In transmission, the scattered intensity increases with etching time as expected from TIS measurements but mainly for small angles. In reflection, the peak for small angles is less developed and the distribution resembles the scattering behavior of a perfect diffuser.

Fig. 5 shows the relative scattering into a certain range derived from figure 4 over the ratio of δ_{rms} roughness to wavelength. This plot clearly shows that with increasing ratio δ/λ the portion of light scattered into small angles increases accordingly. Further investigation of the wavelength dependent angles resolved scattering have shown that especially the diffused scattered fraction in small angles increases with decreasing wavelength of the incident light (not shown here). This result in combination with the results of Figure 4 and Figure 5 shows that different scattering processes with various efficiencies take place.

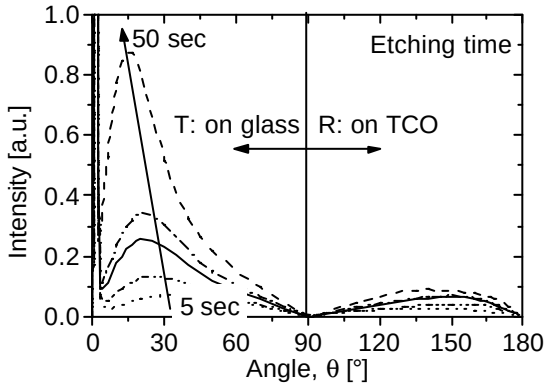

Fig. 4: Transmitted angle dependent scattering intensity of the ZnO etching series for (λ=684nm).

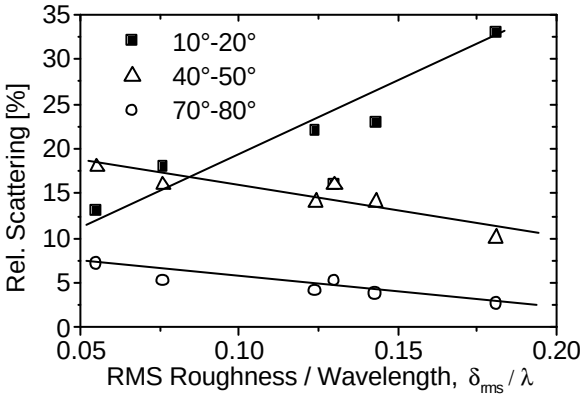

Fig. 5: Transmitted intensity per solid angle versus the scattering angle for glass/rough ZnO (λ=684nm).

3.3 Solar cell characterization

The ZnO substrate etching series was used as front TCO for microcrystalline pin-type diodes with a thickness of 1 µm. Table 2 shows the light I-V parameters of the realized thin film solar cells. The most interesting parameter regarding this work is the short-circuit-current J_{SC}. The improvement in J_{SC} from a smooth to a textured substrate is very distinct.

The gain due to enhanced absorption is around 50%. However, the difference among the solar cells on textured substrates is marginal. The solar cells exhibit a strong decrease in efficiency as a result of a decrease in fill factor and open-circuit-voltage with increasing etching time and root mean square roughness which can be attributed to micro-shunts.

Table 2 Solar cell output parameters for pin solar cells on differently rough ZnO substrates as a function of the root mean square roughness (δ)

δ (nm)	J_{SC} (mA/cm^2)	V_{OC} (mV)	FF (%)	η (%)
non-textured	14.7	522	71.6	5.49
38	21.0	527	67.4	7.47
52	19.9	493	63.8	6.26
85	20.2	458	58.1	5.38
98	20.8	503	64.0	6.71
124	19.6	437	55.8	4.77

For the solar cells of table 2 the quantum efficiency was measured at -1 V (Figure 6). At a reverse bias of -1.0 V, the short circuit current saturates so that all generated charge carriers are extracted. In accordance with the behavior of the short circuit current, the quantum efficiency seems to be nearly independent of the ZnO etching time. There is only a major difference between smooth (as deposited) and etched substrates. The largest difference in QE is found in the wavelength region between 600 and 900 nm. Despite the distinctly different scattering properties of the substrate, there is no further increase of QE with increasing haze.

A second important optimization criteria of the short circuit current is the reflection of the solar cell, which is shown in Figure 7. Due to the employment of a textured TCO the coupling of the incident light into the solar cell (350 – 600nm) and the light trapping caused by repeated reflected within the multilayer structure (600 - 1200) have been improved in comparison to a structure with a smooth TCO layer. However, the low reflection losses are not totally mirrored in the quantum efficiency. In particular at 800 nm a QE of around 0.4 and reflection of 0.15 is detected indicating that 45% of the incident photons neither contribute to the photo-current nor are reflected. Thus these photons are absorbed in other layers (glass, TCO, doped µc-Si:H layers) and back contact.

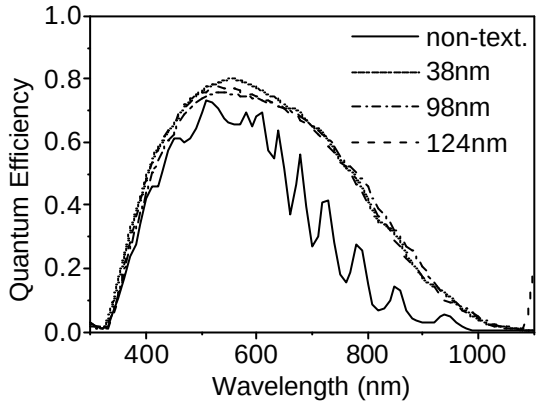

Fig. 6: Quantum efficiency for pin solar cells deposited on differently rough ZnO substrates measured at -1 V.

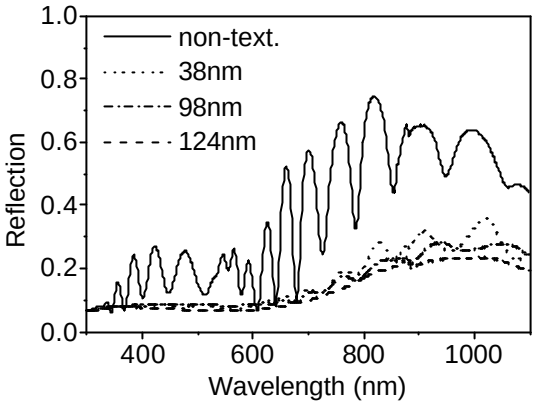

Fig. 7: Reflection of pin solar cells deposited on differently rough ZnO substrates.

The optoelectronic properties of nip-type solar cells were also studied. The difference of the nip- to the pin-structure is that the incident light passes through an about 100 nm thick front TCO-layer instead of passing through a 1-3 mm thick glass and a TCO with a thickness of typically several 100 nm. The nip solar cells were deposited on a highly reflecting back reflector consisting of a glass/$TCO_{textured}$/Ag/TCO layer sequence.

The solar cell output parameters of the realized nip cells are shown in table 3. In order to demonstrate the effect of a highly reflecting back contact also a structure on a substrate coated with a chromium layer was prepared. Due to the low reflection of light with longer wavelength at the rear contact, the evaluated solar cell parameters reflects the performance of a solar cell when light passes only once through the absorption layer. The solar cell on the chromium substrate shows a significantly lower short-circuit current which underlines the importance of a well designed back reflector.

Table 3 Solar cell output parameters for nip solar cells on differently rough ZnO substrates as a function of the root mean square roughness (δ).

δ (nm)	J_{SC} (mA/cm^2)	V_{OC} (mV)	FF (%)	η (%)
non-textured (on chromium)	10.6	401	66.2	2.8
30	17.5	468	71.7	5.9
105	18.2	477	71.0	6.2

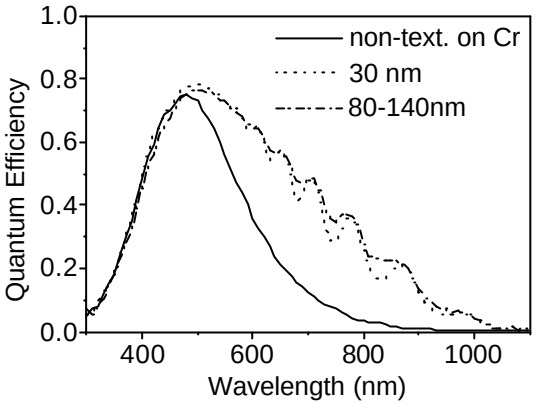

Fig. 8: Quantum efficiency for nip solar cells on differently rough ZnO substrates.

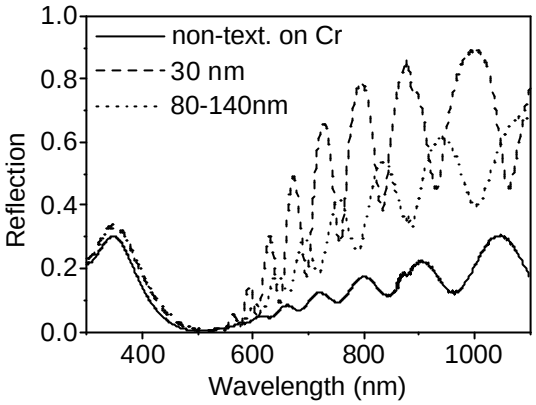

Fig. 9: Reflection for nip solar cells on differently rough ZnO substrates.

Both, the open- circuit voltage and the fill factor of the solar cells increase on a textured back reflector. The short-circuit current of the solar cells with different back contacts is also reflected in the measured QE. The QE values of the cells with textured back reflectors are about 45% at 700nm and 14% at 900nm (Figure 8). The reflection (averaged over the interference structures) amounts to roughly 40% and 65% at wavelengths of 700 and 900nm, respectively (Figure 9).

From these data a loss of 15% and 21% for 700 and 900nm, respectively, is deduced. Consequently, the loss through parasitic absorption, which is not included in the reflection losses, is significantly reduced in nip-cells compared to pin-cells. Due to the thin TCO front contact of the nip structure coupling of light in the solar cell is improved. The reflection of a nip structure at 500 nm is negligible, while the pin structure with a textured front contact exhibits a reflection of around 7.5%. However, light trapping for λ>600nm in nip structures is less effective than in pin structures because interference fringes in the long wavelength range as a consequence of coherent wave propagation can be observed.

Further, the large difference in the Haze functions of the 5 s and 25 s etched substrates is not reflected in the QE measurements. The absolute value of the QE in nip-cells is smaller than in pin solar cells indicating that the smooth air/glass and glass/TCO of the pin structures play an important role on the light trapping due to the total reflection at these flat interfaces.

4. CONCLUSION

The effect of interface roughness (δ_{rms}) of 10 up to 120 nm on the optical properties of microcrystalline pin and nip solar cells was investigated. The various haze (δ_{rms}/λ) measurements of the textured substrates showed the inapplicability of straightforward transmission and reflection coefficients for the whole δ_{rms}/λ. Light trapping in nip structures is less effective than in pin structures. For both structures parasitic absorption reduces the short-circuit current by up to 20%.

The QE of the nip structures shows interference fringes in the long wavelength range as a consequence of coherent wave propagation whereas the QE of pin structures shows similar values without interference fringes for a δ_{rms} exceeding 40 nm.

Acknowledgements: *The authors thank O. Kluth, A. Lambertz, B. Rech, W. Reetz and O. Vetterl for helpful discussions. This work was supported by the Bundesministerium für Bildung und Forschung (BMBF). N. Senoussaoui thanks Deutscher Akademischer Austauschdienst (DAAD) for funding of her stay at Forschungszentrum Jülich.*

REFERENCES

[1] A. Banerjee ans S. Guha, J. Appl. Phys. 69 (1991) 1030

[2] K. Yamamoto, M. Yoshimi, T. Suzuki, Y. Tawada, Y. Okamoto, A. Nakajima, Proc. 2nd World Conference and Exhibition on Photovoltaic Solar Energy Conversion, Vienna, Austria (1998)

[3] F. Leblanc, J. Perrin, J. Schmitt, J. Appl. Phys. 75 (2) (1994) 1074

[4] H. Stiebig, A. Kreisel, K. Winz, M. Meer, N. Schultz, C. Beneking, Th. Eickhoff, H. Wagner, Proc. First World Conference on Photovoltaic Energy Conversion (WCPEC) Hawaii, pp. 603-606 (1994).

[5] A. Löffl, S. Wieder, B. Rech, O. Kluth, C. Beneking, H. Wagner, Proc. 14th European Photovoltaic Energy Conference, pp. 2089-2192 (1997).

[6] O. Kluth, A. Löffl. S. Wieder, C. Beneking, L. Houben, B. Rech, H. Wagner, S. Waser, J.A. Selvan, H. Keppner, Proc. 26th IEEE PVSEC, pp. 715-718 (1997).

[7] H. E. Bennet and J. O. Porteus, J. Opt. Soc. Am. **51**, 123-129 (1961).